# Theranostic Doxorubicin encapsulated FeAu alloy@Metal-organic framework nanostructures enable magnetic hyperthermia and medical imaging in oral carcinoma

Udesh Dhawan [1], Ching-Li Tseng [2,3,4,5], Ping-Hsuan Wu [6], Mei-Yi Liao [7], Huey-Yuan Wang [8,*], Kevin C.-W. Wu [9,10,11,*], Ren-Jei Chung [6,*]

[1] Centre for the Cellular Microenvironment, Division of Biomedical Engineering, School of Engineering, University of Glasgow, Glasgow, G12 8LT, UK

[2] Graduate Institute of Biomedical Materials and Tissue Engineering, College of Biomedical Engineering, Taipei Medical University, Taipei City 110, Taiwan.

[3] International Ph. D. Program in Biomedical Engineering, College of Biomedical Engineering, Taipei Medical University, Taipei City 110, Taiwan.

[4] Research Center of Biomedical Device, College of Biomedical Engineering, Taipei Medical University, Taipei City 110, Taiwan.

[5] International Ph. D. Program in Cell Therapy and Regenerative Medicine, College of Medicine, Taipei Medical University, Taipei City 110, Taiwan.

[6] Department of Chemical Engineering and Biotechnology, National Taipei University of Technology (Taipei Tech), Taipei 106344, Taiwan

[7] Department of Applied Chemistry, National Pingtung University, Pingtung 90003, Taiwan

[8] Department of Stomatology, MacKay Memorial Hospital, Taipei 104217, Taiwan

[9] International Graduate Program of Molecular Science and Technology (NTU-MST), National Taiwan University, Taipei 106216, Taiwan

[10] Department of Chemical Engineering, National Taiwan University, Taipei 106216, Taiwan

[11] Center of Atomic Initiative for New Materials (Al-MAT), National Taiwan University, Taipei 106216, Taiwan

*Corresponding Author: Prof. Dr. Ren-Jei Chung

Email: rjchung@mail.ntut.edu.tw; Tel: (886-2) 2771-2171 ext 2547

Address: Department of Chemical Engineering and Biotechnology, National Taipei University of Technology (Taipei Tech), No. 1, Sec. 3, Zhongxiao E. Rd., Taipei 10608 Taiwan

Also corresponding to Dr. Huey-Yuan Wang (wang461110@yahoo.com.tw) and Prof. Kevin C.-W. Wu (kevinwu@ntu.edu.tw)

Manuscript word count: 7658 words

Number of References: 27

Number of Figures: 7

Number of Tables: 6

## Conflict of Interest

The authors declare that they have no known competing financial interests or personal relationships that could have appeared to influence the work reported in this paper.

## Abstract

Metal-organic frameworks (MOFs) have emerged as attractive candidates in cancer theranostics due to their ability to envelop magnetic nanoparticles, resulting in reduced cytotoxicity and high porosity, enabling chemodrug encapsulation. Here, FeAu alloy nanoparticles (FeAu NPs) are synthesized and coated with MIL-100(Fe) MOFs to fabricate FeAu@MOF nanostructures. We encapsulated Doxorubicin within the nanostructures and evaluated the suitability of this platform for medical imaging and cancer theranostics. FeAu@MOF nanostructures (FeAu@MIL-100(Fe)) exhibited superparamagnetism, magnetic hyperthermia behavior and displayed DOX encapsulation and release efficiency of 69.95% and 97.19%, respectively, when stimulated with alternating magnetic field (AMF). *In-vitro* experiments showed that AMF-induced hyperthermia resulted in 90% HSC-3 oral squamous carcinoma cell death, indicating application in cancer theranostics. Finally, in an *in-vivo* mouse model, FeAu@MOF nanostructures improved image contrast, reduced tumor volume by 30-fold and tumor weight by 10-fold, which translated to enhancement in cumulative survival, highlighting the prospect of this platform for oral cancer treatment.



**Keywords:** metal-organic framework; hyperthermia; iron-gold alloy nanoparticles; cancer theranostics; oral squamous carcinoma

# Graphical Abstract

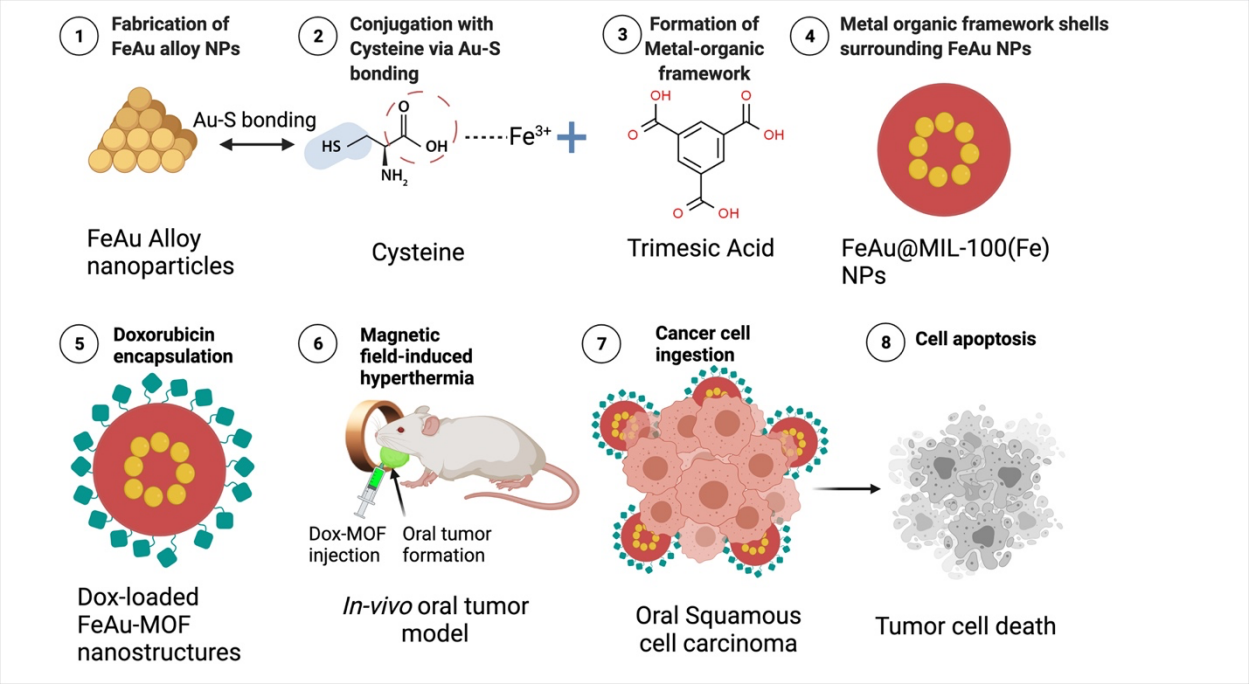


Metal-organic framework-FeAu NPs (MOF-FeAu) nanostructures are fabricated for hyperthermia-induced cancer treatment and imaging. Different shells of MOF were synthesized using cysteine as a linker. An increase in MOF shell number increased biocompatibility and enhanced chemodrug (doxorubicin) encapsulation. In an *in-vivo* mouse model, Doxorubicin-loaded MOF-FeAu nanostructures displayed drastic reduction in tumor size, elevation in survival rate which assistance in tumor imaging

## 1. Introduction

Oral squamous cell carcinoma is one of the most aggressive cancers and is often diagnosed only when it has reached an advanced stage or has metastasized. This characteristic accounts for a poor disease prognosis, with a study reporting the 5-year survival rate close to 27% [1]. To make matters worse, clinical studies have reported a nearly 32% chance of recurrence among survivors, which translates to a 5-year survival rate of only 31% [2]. Due to the drastic survival statistics, various therapeutic strategies have been suggested, including conventional treatments using chemotherapy [3], radiotherapy [4] and surgery [5]. While surgeries fail to eradicate metastasized tumors, chemotherapy and radiotherapy cause severe side effects [6], including damage to healthy tissue surrounding cancer stroma, primarily due to non-specific targeting. Hyperthermia via thermal ablation has emerged as a recent strategy [7]. However, damage to the non-cancerous tissue limits its applications on a wide scale. To minimize damage to the healthy stroma, nanoparticles have been engineered and often employed for selective heating of the diseased tissue through optical or magnetic excitation [8, 9].

Hyperthermia using optical excitation is based on the ability of the nanoparticles to absorb light of specific wavelengths and generate heat, and this methodology is commonly referred to as Photodynamic therapy (PDT) [10]. PDT offers a multitude of benefits such as site-specificity and less invasiveness [9]. However, a key drawback in using PDT for cancer treatment stems from the short diffusion distance limit [11]. Clinically, it translates to the inability of light to penetrate deep tissues where tumors may reside. This makes PDT a rather less attractive candidate for cancer treatment. Thus, it is the need of the scientific community to engineer more comprehensively designed therapeutic routes. An alternative therapy involves using an alternating magnetic field (AMF) to stimulate magnetic nanoparticles to generate heat to achieve local hyperthermia for

cancer cell death. Magnetic hyperthermia (MH) is a fast-evolving, robust and highly effective way to specifically target cancerous tissue [12]. This is achieved by localizing magnetic nanoparticles in the diseased area using an external magnet, followed by stimulation with an AMF which causes cancer cell death via hyperthermia [13]. Besides inducing local hyperthermia, magnetic nanoparticles also offer a myriad of benefits such as ease of functionalization with chemo drugs and serving as imaging agents for better cancer tissue visualization [14]. For instance, we have recently shown that conjugation of Angiopep-2 with nanoparticles facilitates their passage through the blood brain barrier to treat glioma via hyperthermia [9].

Despite numerous advantages, a key drawback of using nanoparticles is their cytotoxicity. Studies have shown that the nanomaterial-based cytotoxicity is not only composition-dependent, but also shape and size-dependent [15]. To enhance biocompatibility, magnetic nanoparticles are often coated with nanocarriers such as polymers [16], liposomes [17], dendrimers [18]. These organic coatings not only enhance the biocompatibility, but also enable encapsulation of chemodrugs that can be released on-demand. Systematically, once the encapsulated drug-nanoparticle combination reaches the site of interest, hyperthermia dissociates the nanocarrier, resulting in effortless release of drug-conjugated nanoparticles. The chemodrug-conjugated nanoparticles also possess an additional benefit as recent studies have shown that an increase in the surrounding temperature sensitizes cancer cells to chemo and radio treatment [19]. Thus, on one hand magnetic hyperthermia can cause cellular protein damage and direct cancer cell death and on the other hand make the cancer stroma more sensitive to chemo or radiotherapy. It is for this this reason that hyperthermia and chemotherapy treatments are often given within an hour of each other.

Metal organic frameworks (MOFs) represent self-assemblies of metal ions and organic ligands via coordination bonds and have also emerged as attractive drug delivery platforms for

anti-cancer therapy owing to large surface area, high stability, tunable size and ease of functionalization [20, 21]. These properties make MOFs highly suitable for drug encapsulation and controlled release. Mesoporous iron (III) Trimesate (MIL-100), represents a MOF in which trimesic acid ($H_3BTC$) acts as the organic ligand and iron (III) ions act as the coordination center. It displays a pore diameter of 3.9 nm coupled with a large surface area (2000 $m^2g^{-1}$) and high biocompatibility, making it an ideal candidate for drug nanocarrier. While applications of MIL-100 MOF have been extensively studied in PDT [22, 23], however, little research has been done on exploring its applications in magnetic hyperthermia for cancer treatment. Furthermore, there is little to no evidence on strategies to precisely control the amount of drug encapsulated within the MOF. A highly effective anti-cancer platform must exhibit high biocompatibility along with site-specific targeting and on-demand drug release and magnetic nanoparticles and chemodrug encapsulated within the MOF accurately represent one such platform.

In this study, we report the fabrication of MIL-100 MOF as a drug delivery platform for limiting oral cancer growth via generation of magnetic hyperthermia. We used Cysteine as a linker to fabricate FeAu@MIL-100(Fe) MOF with varying shell number. We studied the biocompatibility of this platform among various cell lines as a function of MOF shells followed by dissociation via hyperthermia to target cancer growth for application in cancer therapeutics. Briefly, this study reports: (a) encapsulation and release efficiency of doxorubicin, as a function of FeAu@MIL-100(Fe) MOF shell number, (b) effect of FeAu@MIL-100(Fe) MOF shell number on cell viability upon magnetic stimulation using *in-vitro* models, (c) application of this platform in medical imaging as a contract agent and (d) efficacy of this platform in attenuating oral cancer growth via administration of magnetic hyperthermia in an *in-vivo* mouse model. The MOF nanocarrier platform developed in this study exhibits high biocompatibility while simultaneously

eradicating oral cancer growth along with serving as an imaging agent. Application of this multimodal platform are expected in the fields of nanotheranostics, nanobiotechnology, and cancer therapeutics.

## 2. Methods

### 2.1 Synthesis and Characterization of FeAu Nps

FeAu alloy nanoparticles were synthesized via pyrolysis following the methodology previously reported [8]. Briefly, Ferrous sulfate heptahydrate ($FeSO_4.7H_2O$) and tetrachloroauric (III) acid trihydrate ($HAuCl_4.3H_2O$) as precursors. Toluene, sodium borohydride ($NaBH_4$) and dodecyl dimethyl ammonium bromide (DDAB) were used as solvent, reducing agent and surfactant, respectively. 0.064 g DDAB was dissolved in 20 mL toluene, added to a three-necked flask and passed over argon to remove residual oxygen. The mixture was heated to 110°C with constant stirring for 15 minutes. 0.012 g $FeSO_4.7H_2O$, dissolved in 1mL DI water was added to the flask, followed by addition of $NaBH_4$ (0.03M). This mixture was stirred magnetically for 20 minutes. To reduce gold chloride to gold, 0.212 g sodium 3-mercapto-1-propanesulphonic acid was then mixed with $HAuCl_4.3H_2O$ followed by simultaneous addition of $NaBH_4$. The mixture was stirred for 30 minutes and 1 mL $NaBH_4$ (0.03M) was added to the mixture in the final step. The temperature was maintained at 84°C for three hours. The resulting solution was centrifuged at 9000 rpm for 10 minutes and nanoparticles were collected using a magnet, washed several times with ethanol and dried under vacuum. Morphology of nanoparticles was analyzed using Transmission electron microscope (TEM) and nanoparticle size was quantified using Image J. The composition of nanoparticles was analyzed using Energy dispersive X-ray spectroscopy (EDS) and X-ray diffraction (XRD). Finally, the magnetic properties of nanoparticles were confirmed via SQUID.

## 2.2 Synthesis of cysteine functionalized FeAu NPs

To functionalize nanoparticles, 0.216 g cysteine and 1mL NaOH were added to 30mL DI water. 50mg FeAu Nps were added to this solution and subjected to overnight stirring at room temperature. The solution was centrifuged the following day followed by several washings in Ethanol. Cysteine-functionalized Nps (FeAu-Cys) were characterized using Zetasizer and dispersed in ethanol for further use.

## 2.3 Synthesis and characterization of FeAu@MIL-100(Fe) NPs with different number of shells

FeAu@MIL-100(Fe) core-shell nanostructures were fabricated via self-assembly. 20 mg FeAu-Cys were first dispersed in 13.2 mL $FeCl_3.6H_2O$ ethanol solution under ultrasound treatment for 20 minutes. The resulting solution was centrifuged and washed using ethanol. The products were then mixed with trimesic acid and heated to 70°C in a water bath for 30 minutes. This procedure was referred to as one cycle. FeAu-MIL-100(Fe) with different MOF shells were synthesized following 5 or 10 cycles. The resulting MOF nanostructures were morphologically characterized using TEM and the thickness was quantified using Image J. The formation of MOF nanostructures was confirmed using Fourier transfer infrared spectroscopy (FTIR), Dynamic light scattering (DLS), the composition was analyzed using EDS and magnetic properties were studied using SQUID.

## 2.4 Encapsulation and release of doxorubicin from MOF nanostructures

10 mg FeAu@MIL-100(Fe) with 5 or 10 shells were first dispersed in 10 mL PBS, followed by addition of 0.001 g doxorubicin. The solution was stirred at room temperature for 24 hours. DOX-loaded FeAu@MIL-100(Fe) NPs were collected via centrifugation. Absorbance at 480 nm using ultraviolet visible (UV) UV-Vis spectrophotometry was measured and the standard curve was plotted using the following equation:

$$\text{Dox A}(480\text{ nm}) = 1.736C + 0.0122$$

The loading efficiency was calculated using the following equation:

$$Drug\ loading\ percentage\ (DLP\ \%) = \frac{M0 - Mf}{M0} x100$$

Where M0 is the initial mass of the drug in the solution, Mf is the mass of drug in the final supernatant. To calculate the drug release efficiency, FeAu@MIL-100(Fe)-Dox NPs with 5, 10 shells at a known concentration of 5 mg/mL were first dispersed in DI water, and then poured into a 35 mm dish attached to high frequency induction waves (HFIW) set-up (700 – 1000 KHz) followed by stimulation for 5 or 10 minutes. To estimate the drug release due to orbital shaking, an additional experimental group was included in which Dox-loaded nanostructures were subjected to 50 rpm shaking for 5 or 10 minutes. The solution from both experimental groups was collected via centrifugation and the absorbance was measured at 480 nm. The standard curve was plotted using the equation mentioned above and the release profile was calculated using the following equation:

$$Drug\ release\ percentage\ (DRP\ \%) = \frac{Mf}{Mdl} x100$$

Where Mf is the mass of the drug in the solution and Mdl is the mass of drug loaded in the nanoparticles.

**2.5 Hyperthermia induction upon magnetic stimulation**

To study the efficiency of FeAu, MIL-100 (Fe) and FeAu@MIL-100(Fe) NPs (5, 10 shells) to induce hyperthermia, all experimental groups were first dispersed in water at an identical concentration of 5 mg/mL and subjected to high frequency induction heating (HFIH, 700 – 1000 KHz) and the solution temperature was recorded every 30 seconds for 5 minutes.

**2.6 Cell culture**

L929 cells (mouse fibroblasts, ATCC, USA) were cultured in DMEM whereas HSC-3 (human tongue squamous carcinoma, ATCC, USA) were cultured in MEM supplemented with 10% fetal bovine serum (FBS, GIBCO, USA), 100 U/mL penicillin and 100 µg/mL streptomycin, cultured in T75 cell culture flasks and incubated at 37 ºC, 5% $CO_2$ and 95% humidity.

**2.7 In-vitro cytotoxicity analysis**

The cytotoxicity of FeAu and FeAu@MIL-100(Fe) NPs with different shell number was evaluated using L929 (fibroblasts) and HSC-3 (oral squamous carcinoma) as model cell lines. Cells were cultured at a density of 1 x $10^5$ cells/mL in 96 well plates, divided into four experimental groups were allowed to attach. The four experimental groups included blank (media only, negative control), FeAu NPs, FeAu@MIL-100(Fe) NPs with 5 shells and FeAu@MIL-100(Fe) NPs with

10 shells. The cytotoxicity of FeAu and FeAu@MIL-100(Fe) NPs (5, 10 shells) was evaluated at concentrations of 31.25, 62.5, 125, 250 and 500 µg/mL. Each experimental group comprised of five replicates. After 24 hours of incubation, culture media was aspirated and cells were washed with 200 µL PBS. 200 µL of culture media containing MTT reagent was then added to each well and samples were incubated for four hours in dark. After designated time period, culture media was aspirated and replaced with 200 µL DMSO. Culture dishes were placed on a rotary shaker for 10 minutes at 150 rpm to dissolve formazan crystals. Absorbance was measured at 570 nm using an ELISA reader and data was expressed as cell viability.

**2.8 In-vitro analysis of magnetic-stimulation-generated hyperthermia**

To evaluate the ability of FeAu@MIL-100(Fe) NPs in limiting cancer cell growth via magnetic field-induced hyperthermia, HSC-3 (oral squamous carcinoma) cells were used as a model. Specifically, HSC-3 cells were first seeded at a density of 3 x $10^5$ cells/mL in 35mm culture plates and allowed to attach for 24 hours. Three experimental groups comprising of FeAu, FeAu@MIL-100(Fe) NPs with 5 shells and FeAu@MIL-100(Fe) NPs with 10 shells were used for this experiment. The experimental groups were first sterilized using UV light for 30 minutes and then dissolved in MEM culture media at a concentration of 100 µg/mL and 1 mL was added to culture plates. After 4 hours of incubation, the samples were subjected to HFIW for 10 minutes. Each experimental group comprised of three replicates. The samples were then placed in the incubator. After 24 hours, cell viability was assessed using MTT assay following the protocol mentioned above.

**2.9 In-vivo mouse model to evaluate hyperthermia-mediated anti-cancer activity**

15 male Balb/c nude mice (4-6 weeks old, weight 18-22 g) purchased from BioLASCO Co., Ltd. (Taipei, Taiwan) were employed for this study. The animals were acclimatized for at least one week prior to the experiment. The experiments were carried out at MacKay Memorial Hospital with their guidelines to care and use of animals. All protocols for animal study and use were approved by affiliated Institutional Animal Care and Use Committee (IACUC) under the affidavit no. MMH-A-S-108-16. The animals had ad libitum access to standard rat chow and water at all times. For surgical anesthesia, zoletil 50 (Virbac, France) was injected intraperitoneally at a dosage of 20 mg/Kg. Subcutaneous tumors were formed by injecting HSC-3 cells (2 x $10^6$ cells/mouse) into the right forelimb. When the tumor diameters reached 5 mm, the mice were divided into three groups: Control (200 µL), FeAu@MIL-100(Fe)-Dox NPs 5 shells (200 µL MEM 250 µg/mL) and FeAu@MIL-100(Fe)-Dox NPs 10 shells (200 µL MEM 250 µg/mL). After 2 hours of cellular uptake, the right forelimb was subjected to HFIW (700 – 1000 KHz) for 10 minutes to administer hyperthermia treatment. The tumor size was measured every 3 days for 21 days. Tumor volume was calculated using the following formula: $a \times b^2 \times 0.5$, where a is the largest diameter and, b is the smallest diameter. Each group comprised of 5 biological replicates.

**2.10. Immunohistochemical analysis**

Immunohistochemical analysis was performed to assess safety of the metal-organic framework nanotheranostics platform developed in this study. For this, tissues from major organs including heart, liver, lungs, spleen and kidneys were dissected from mice in control and treatment groups, followed by fixation in 10% formalin and paraffin embedding. The tissues were then cut into 5-mm thin slices and stained with Hematoxylin & Eosin (H&E).

## 2.11. Statistical analysis

All experiments were performed at least thrice and the data was represented as mean with standard deviations. Statistical analysis was performed to identify datasets that significantly differed from each other. Statistical analysis was performed using Kruskal-Wallis test with Dunn's multiple comparisons or One-Way ANOVA in GraphPad Prism 9. The p-value was set at $\leq 0.05$. * represents datasets with p-value $\leq 0.05$ and ** represents datasets wit p-value $\leq 0.01$.

# 3. Results and Discussions

## 3.1 Characterization of FeAu alloy nanoparticles

The nanoparticle size and morphology can regulate its hyperthermia ability, making these parameters crucial for characterization [24]. In this study, the nanoparticle morphology was characterized using TEM, size of nanoparticles was measured using Image J and the composition was analyzed using energy-dispersive X-ray spectroscopy (EDS). The TEM analysis revealed that FeAu nanoparticles (FeAu NPs) displayed a round morphology with an average size of 8.38 nm (Figure 1a, b). The EDS analysis confirmed that the nanoparticles comprised mainly of iron and gold (Figure 1c). The weight percentage of iron and gold was 23.23 and 76.77%, respectively, while the atomic percentage of iron and gold was 51.62 and 48.38%, respectively (Table 1). Thus, iron and gold were present in approximately 1:1 ratio. Collectively, these results confirmed the formation of FeAu nanoparticles. Importantly, TEM analysis did not reveal presence of core-shell structure, confirming that the synthesized nanoparticles were alloy nanoparticles. We then characterized the crystal structure of FeAu NPs using X-ray diffraction which highlighted the 2θ peaks at 44.42 and 64.56° which correspond to (110) and (200) body-centered cubic iron (Figure 1d). Furthermore, the 2θ peaks at 44.48 and 64.72° correspond to (200) and (220) face center cubic gold particles. These results are consistent with our previously study in which we reported the synthesis of 7.2 nm sized spherical FeAu alloy nanoparticles [8]. Collectively, these findings confirmed the presence of iron and gold in the nanoparticles.

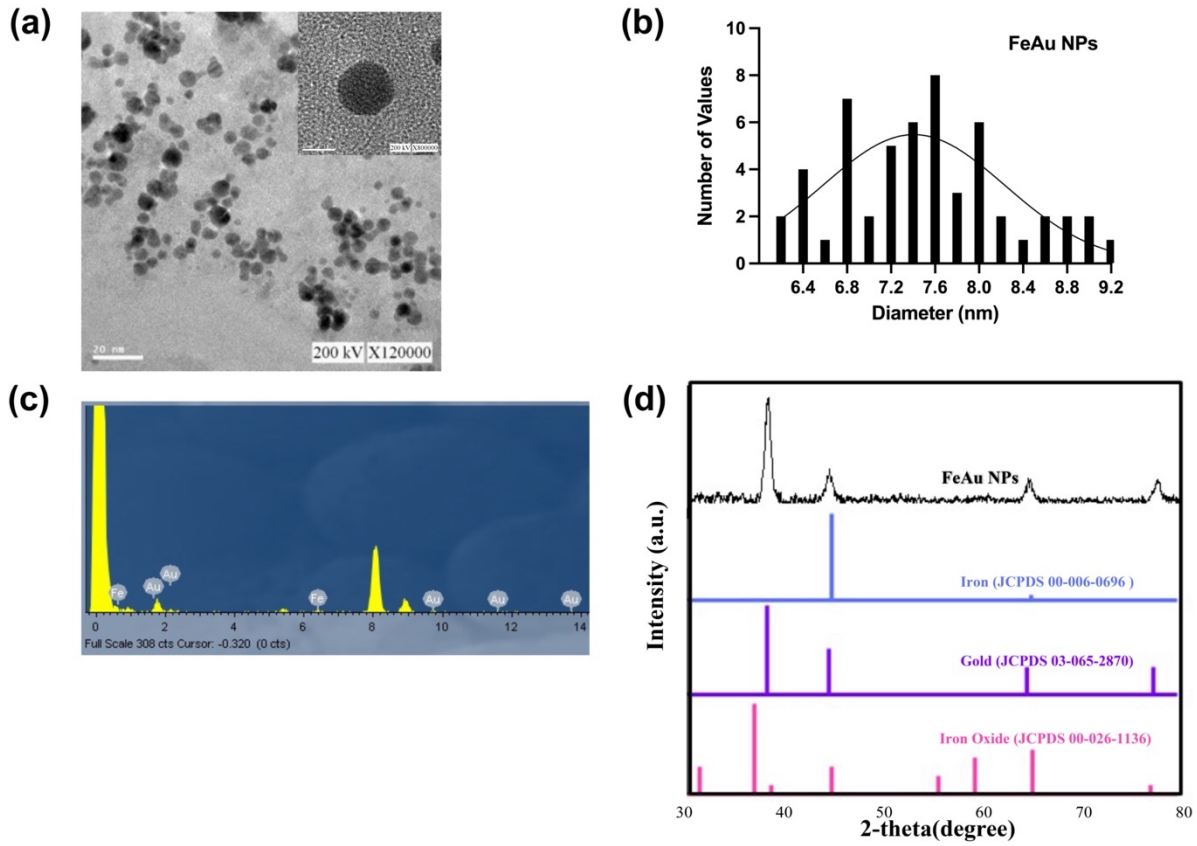


**Figure 1. Characterization of Iron-gold alloy nanoparticles (FeAu NPs). (a)** Transmission electron micrographs (TEM) of FeAu NPs. The magnification is 120000X and scale bar = 20 nm. Inset shows high-magnification of FeAu NPs. The magnification is 800000X and scale bar = 5 nm. **(b)** Size distribution of FeAu NPs. X-axis represents diameter and y-axis represents frequency. **(c)** Energy dispersive x-ray spectroscopy of FeAu NPs to analyze FeAu NPs composition. **(d)** Characterization of FeAu NPs using X-ray diffraction. The peaks correspond to 2-theta values which represent different lattices of the FeAu NPs.

**Table 1. EDS analysis of FeAu NPs**

| Element | Weight (%) | Atomic (%) |
|---|---|---|
| Fe | 23.23 | 51.62 |
| Au | 76.77 | 48.38 |

### 3.2 Characterization of FeAu@MIL-100(Fe) nanostructures

We first performed TEM analysis of FeAu@MIL-100(Fe) 5 shell nanostructures to visually inspect the presence of MIL-100(Fe) which revealed that FeAu NPs were covered with a thin MIL-100(Fe) layer, resulting in the formation of core-shell nanostructures (Figure 2a). The particle size was found to be 129.86 nm (Figure 1c) and the shell thickness was measured to be 8.38 nm (Table 3). We then performed TEM analysis of FeAu@MIL-100(Fe) 10 shell nanostructures and hypothesized that an increase in the number of shells would result in larger particle size and thicker shell (Figure 2b). Consistent with our hypothesis, TEM analysis highlighted that FeAu@MIL-100(Fe) 10 shell nanostructures were 245.76 nm in size (Figure 2d, Table 3). Furthermore, nearly 4-fold increase (38.49 nm) in shell thickness was also observed. Collectively, these results confirmed that FeAu@MIL-100(Fe) nanostructures display a core-shell morphology. Elemental analysis of FeAu@MIL-100(Fe) 10 shell nanostructures using EDS revealed that the weight percentage of Fe and Au in the nanostructures was 100 and 0% (Table 2). Similar results were obtained when atomic percentages of both elements were compared. The difference in elemental composition can be explained on the basis of core-shell nanostructure

formation. Consequently, the presence of iron can be attributed to the presence of MIL-100(Fe) shell that covers FeAu nanoparticles.

The formation of FeAu@MIL-100(Fe) complex was confirmed using Fourier transform infrared spectroscopy (FTIR) (Figure 2e). We first performed FTIR analysis of FeAu NPs which revealed absence of any major functional groups. This was followed by analysis of pure MIL-100(Fe) which displayed peaks at 1629 and 1380 $cm^{-1}$ which can be attributed to -COO stretch. Furthermore, the emergence of sharp peaks at 760 and 710 $cm^{-1}$ represents -C=O functional group (Figure 2e). These peaks were used as a reference and FTIR analysis was again performed after coating FeAu@MIL-100(Fe) NPs with 5 and 10 shells. As shown in figure 2e, FeAu@MIL-100(Fe) NPs with 5 displayed identical peaks as pure MIL-100(Fe) but with reduced signal intensity. However, the peak intensity increased after coating 10 shells, indicating that MIL-100(Fe) forms a coating outside FeAu NPs. This core-shell nanostructure was also confirmed via TEM and EDS analysis. TEM.

To enable formation of multi-shell nanostructures and entrapment of doxorubicin, FeAu NPs were first conjugated with Cysteine (via Au-S bond) which imparts negative charge to the nanoparticles due to the presence of carboxylic groups, enabling the formation of MIL-100 (Fe) shells due to the presence of $Fe^{3+}$ ions (Figure 2f). Cysteine was preferred over thioglycolic acid for this purpose due to its higher biocompatibility. The conjugation of cysteine with FeAu NPs was confirmed using Zetasizer. The zeta potential of Cys-FeAu NPs was -18.53±0.8mV but increased to -13.33±0.5 which can be attributed to the presence of $Fe^{3+}$ ions (Figure 2f). The zeta potential then slightly decreased to -14.6±0.7 after formation of a single layer of MIL-100(Fe) which can be attributed to the presence of -COO- groups in Trimesic acid (Figure 2f). In summary,

these experimental confirmed the successful conjugation of cysteine to FeAu NPs which then facilitated the formation of FeAu@MIL-100(Fe) nanostructures.

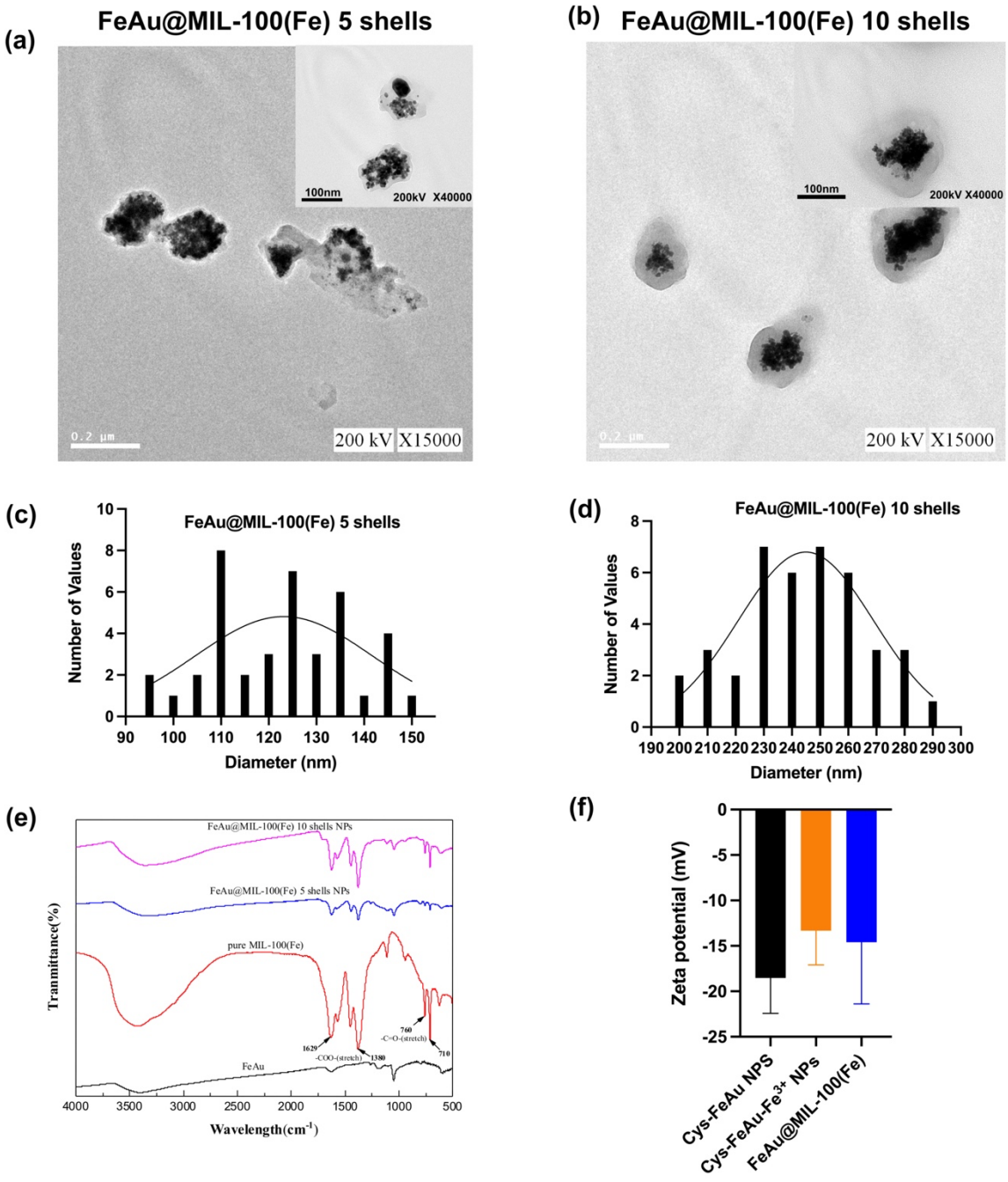

**Figure 2. Characterization of FeAu@MOF nanostructures with different shells. (a)** TEM micrographs of FeAu@MIL-100(Fe) 5 shells nanostructures. The magnification is 15000X and scale bar = 200 nm. The inset shows high-magnification image. The magnification is 40000X and scale bar = 100 nm. **(b)** TEM micrographs of FeAu@MIL-100(Fe) 10 shells nanostructures. The magnification is 15000X and scale bar = 200 nm. The inset shows high-magnification image. The magnification is 40000X and scale bar = 100 nm. **(c, d)** Size distribution of FeAu@MIL-100(Fe) 5 and 10 shells nanostructures. **(e)** Fourier transform infrared spectrum of FeAu NPs as well as FeAu@MOF nanostructures. The peaks corresponding to specific functional groups present in MOF-conjugated FeAu NPs confirmed successful formation of FeAu@MOF nanostructures. **(f)** Confirmation of FeAu@MOF nanostructure formation using Zetasizer. The y-axis represents zeta potential and x-axis represents experimental groups.

**Table 2. EDS analysis of FeAu@MIL-100(Fe) 10 shell nanostructures**

| **Element** | **Weight (%)** | **Atomic (%)** |
|---|---|---|
| Fe | 100 | 100 |
| Au | 0 | 0 |

**Table 3. Analysis of FeAu@MIL-100(Fe) 5 and 10 shell nanostructures**

| **Experimental group** | **Particle size (nm)** | **Shell thickness (nm)** |
|---|---|---|
| FeAu@MIL-100(Fe) 5 shells | 129.86 | 8.38 |
| FeAu@MIL-100(Fe) 10 shells | 245.76 | 38.49 |

### 3.3 Assessing magnetic properties and hyperthermia ability of FeAu@MIL-100(Fe) nanostructures

The magnetization extent of pure MIL-100 (Fe), FeAu NPs and FeAu@MIL-100(Fe) 10 shell nanostructures was assessed from -20,000 to 20,000 G in the presence of the magnetic field at the temperature of 300K. Despite possessing iron ions, pure MIL-100(Fe) did not display any magnetic strength and its saturation magnetization was 0.24 emu/g (Figure 3a). This observation highlights its unsuitability for magnetothermal therapy. The hysteresis curve of FeAu NPs and FeAu@MIL-100(Fe) passed through the origin, highlighting the superparamagnetic nature. The saturation magnetization (M) of FeAu NPs was 10.87 emu/g but dropped to 7.44 emu/g in FeAu@MIL-100Fe 10 shell nanostructures which can be attributed to the presence of 10 shells around FeAu NPs (Figure 3a, Table 4). Nevertheless, as shown by our previous studies as well as by other groups, nanoparticles with even saturation magnetization as low as 3.5 emu/g can be used for hyperthermia treatment [16].

Based on these findings, we then decided to directly assess the ability of FeAu@MIL-100 (Fe) 5 and 10 shell nanostructures to generate hyperthermia. Previous studies have shown that cancer cells suffer apoptosis at a lower temperature (39-43°C) as compared to healthy cells (46°C). This provides researchers with an opportunity to specifically target cancer stroma using hyperthermia. To evaluate suitability of nanostructures synthesized in this study for magnetothermal therapy, we tested the ability of 5 mg/mL FeAu NPs, FeAu@MIL-100 (Fe) 5 and 10 shell to raise solution temperature in the presence of high frequency induction waves (HFIW, 700-1100 KHz) over a period of 600 seconds. The temperature was recorded every 30 seconds. Consistent with the results in our previous study [8], FeAu NPs displayed remarkable hyperthermia

ability and triggered a consistent increase in solution temperature with time, maximizing at 48.5°C (Figure 3b). Furthermore, the hyperthermia ability of FeAu@MIL-100 (Fe) 5 and 10 shell nanostructures was lower as compared to pure FeAu NPs due to the presence of MOF shells surrounding the nanoparticles. Nevertheless, the temperature for 5 and 10 shell nanostructures reached 43.2 and 41.1°C which is expected to be sufficient to target cancer cells (Figure 3b). Noteworthy, despite addition of 5 extra shells (as compared to FeAu@MIL-100 (Fe) 5 shell), the difference in temperature was merely 2.1°C (Figure 3b). Collectively, these results highlight the suitability of FeAu@MOF nanostructures for magnetothermal therapy.

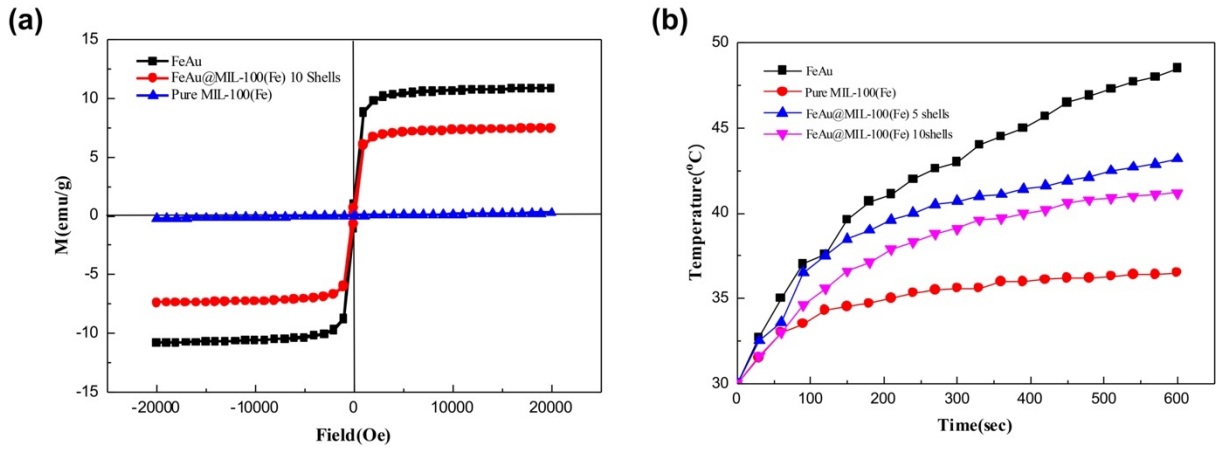


**Figure 3. Analysis of magnetic and hyperthermia properties of FeAu NPs and FeAu@MOF nanostructures. (a)** M-H curves of FeAu NPs and FeAu@MOF nanostructures highlighting that FeAu@MOF nanostructures displayed a saturation magnetization of 6 emu/g. The saturation magnetization decreased after encapsulation of FeAu NPS within the MOF **(b)** Confirmation of hyperthermia ability of FeAu NPs and FeAu@MOF nanostructures with 5 or 10 shells. The x-axis represents time in seconds and y-axis represents temperature in Celsius.

**Table 4. Measurement of saturation magnetization of FeAu NPs and FeAu@MOF nanostructures**

| Experimental Group | Saturation magnetization (emu/g) |
|---|---|
| FeAu NPs | 10.87 |
| FeAu@MIL-100(Fe) 10 shells | 7.44 |
| Pure MIL-100 (Fe) | 0.24 |

### 3.4 Evaluation of Doxorubicin encapsulation and release

It has now been well established that exposure to hyperthermia sensitizes cancer cells to chemotherapy and for this reason a plethora of studies have reported fabrication of drug-encapsulating polymeric nanoparticles. The presence of 5 and 10 shells of MOF around FeAu NPs provided us with an opportunity to encapsulate doxorubicin within the shells followed by hyperthermia-induced release. We hypothesized that an increase in the number of shells (from 5 to 10) will not only improve the biocompatibility of FeAu@MOF nanostructures, but also increase its encapsulation efficiency. Furthermore, we also hypothesized that hyperthermia generation may result in dissociation of MOF shells, resulting in doxorubicin release. A previous study has reported that pure MIL-100(Fe) displays 73.6% doxorubicin encapsulation [25]. To assess the ability of the FeAu@MOF nanostructures for doxorubicin encapsulation, we incubated doxorubicin with FeAu@MIL-100 (Fe) 5 and 10 shell nanostructures under constant stirring for 24 hours. We observed that the encapsulation efficiency of FeAu@MIL-100 (Fe) 10 shell nanostructures was 69.956% which is very similar to that of pure MIL-100(Fe) (Table 5). Furthermore, the 5 shell

nanostructures displayed the loading efficiency of 54.18%. We then set out to investigate if hyperthermia treatment can result in doxorubicin release and observed that 99.17% of doxorubicin could be released when FeAu@MIL-100 (Fe) 10 shell nanostructures were subjected to HFIW for 10 minutes (Table 5). In contrast, FeAu@MIL-100 (Fe) 5 shell nanostructures displayed a 38% release efficiency. Furthermore, we also tested if doxorubicin can be released from the nanostructures in the absence of hyperthermia and found that after 10 minutes of stirring using an orbital shaker resulted in 4.33 and 6.56% release of encapsulated drug from 5 and 10-shell nanostructures, respectively (Table 6). The higher number of shells (10 shells) are expected to deliver higher chemodrug load at the tumor site. Collectively, these results highlight the suitability and potential of FeAu@MOF nanostructures to encapsulate chemodrugs followed by stimulated release via hyperthermia for cancer therapy.

**Table 5. Doxorubicin encapsulation and release efficiency**

| Experimental group | Loading efficiency (%) | Release efficiency % (5 Min) | Release efficiency % (10 Min) |
|---|---|---|---|
| FeAu@MIL-100 (Fe) 5 shell + HFIW | 54.18 | 18.87 | 38.00 |
| FeAu@MIL-100 (Fe) 10 shell + HFIW | 69.95 | 64.59 | 97.19 |

**Table 6. Doxorubicin release under orbital shaker stimulation**

| Experimental group | Release efficiency (%) |
|---|---|
| FeAu@MIL-100 (Fe) 5 shell + 50 rpm | 4.33 |
| FeAu@MIL-100 (Fe) 10 shell + 50 rpm | 6.56 |

469

470 **3.5 Hyperthermia-induced oral squamous cancer cell death**

471 We then decided to evaluate the cytotoxicity of FeAu NPs and FeAu@MIL-100 (Fe) 5 and
472 10 shell nanostructures by incubating cells in varying concentration of FeAu NPs (31.25 to 500
473 µg/mL). MTT assay was performed to assess cytotoxicity which highlighted that at 31.25 µg/mL
474 concentration of FeAu NPs, the viability of L929 fibroblasts was maintained at 83%. In contrast,
475 FeAu@MIL-100 (Fe) 5 shell nanostructures displayed higher cell viability (90%) which can be
476 due to the presence of MOF shells surrounding the nanoparticles (Figure 4b). Furthermore, cells
477 incubated with FeAu@MIL-100 (Fe) 10 shell nanostructures displayed even higher cell viability
478 (95%). Collectively, these result point towards the elevated biocompatibility due to the presence
479 of MOF shells. Expectedly, cell viability decreased with an increase in the nanoparticle
480 concentration (Figure 4b). However, at all concentrations, FeAu@MIL-100 (Fe) 10 shell
481 nanostructures displayed the highest cell viability. Interestingly, at 31.25 µg/mL FeAu NPs
482 concentration, HSC-3 oral squamous cancer cells displayed higher cytotoxicity towards the FeAu
483 NPs (cell viability <80%, Figure 4c). Noteworthy, from 62.5 to 500 µg/mL FeAu NPs
484 concentration, HSC-3 cells displayed higher cell viability as compared to L929 fibroblasts,
485 however, this difference was not statistically significant. We did not observe any qualitative
486 difference in the amount of FeAu NPs, FeAu@MIL-100 (Fe) 5 and 10 shell nanostructures within

the cells as observed via optical microscopy (Figure 4a). Consequently, we did not observe any significant difference in cytotoxicity between 62.5 to 500 µg/mL FeAu NPs, FeAu@MIL-100 (Fe) 5 and 10 shell nanostructures (Figure 4c). Based on this finding we decided to use 100 µg/mL for the subsequent experiments.

Collectively, our results so far confirmed that FeAu@MIL-100 (Fe) 5 and 10 shell nanostructures display superparamagnetic behavior with an ability to generate hyperthermia upon HFIW stimulation. Furthermore, FeAu@MIL-100 (Fe) 10 shell nanostructures also displayed highest doxorubicin encapsulation and release. These findings motivated us to assess if a higher amount of chemodrug encapsulation translates to an elevated cell death via hyperthermia. Our results show that after 5 minutes of HFIW stimulation, HSC oral squamous cancer cells displayed significant reduction in cell viability as compared to the experimental groups without any treatment. The cell viability of FeAu@MIL-100(Fe) 5 shell experimental group dropped from 63 (no treatment) to 32% (Figure 4d). Additionally, cells incubated with FeAu@MIL-100 (Fe) 10 shell experimental group displayed an even lower viability (14%) which can be attributed to the higher release of doxorubicin due to hyperthermia. After 10 minutes of HFIW stimulation, highest cytotoxicity was displayed by FeAu@MIL-100(Fe) 10 shell nanostructures, suggesting their application in cancer theranostics (Figure 4d). Previous research has shown that hyperthermia-mediated cellular apoptosis is triggered via TNF-α signaling pathway in glioblastoma[26, 27]. However, a comprehensive analysis of gene and molecular perturbations in oral cancer cells in response to magnetic hyperthermia is still unknown and is beyond the focus of this study.

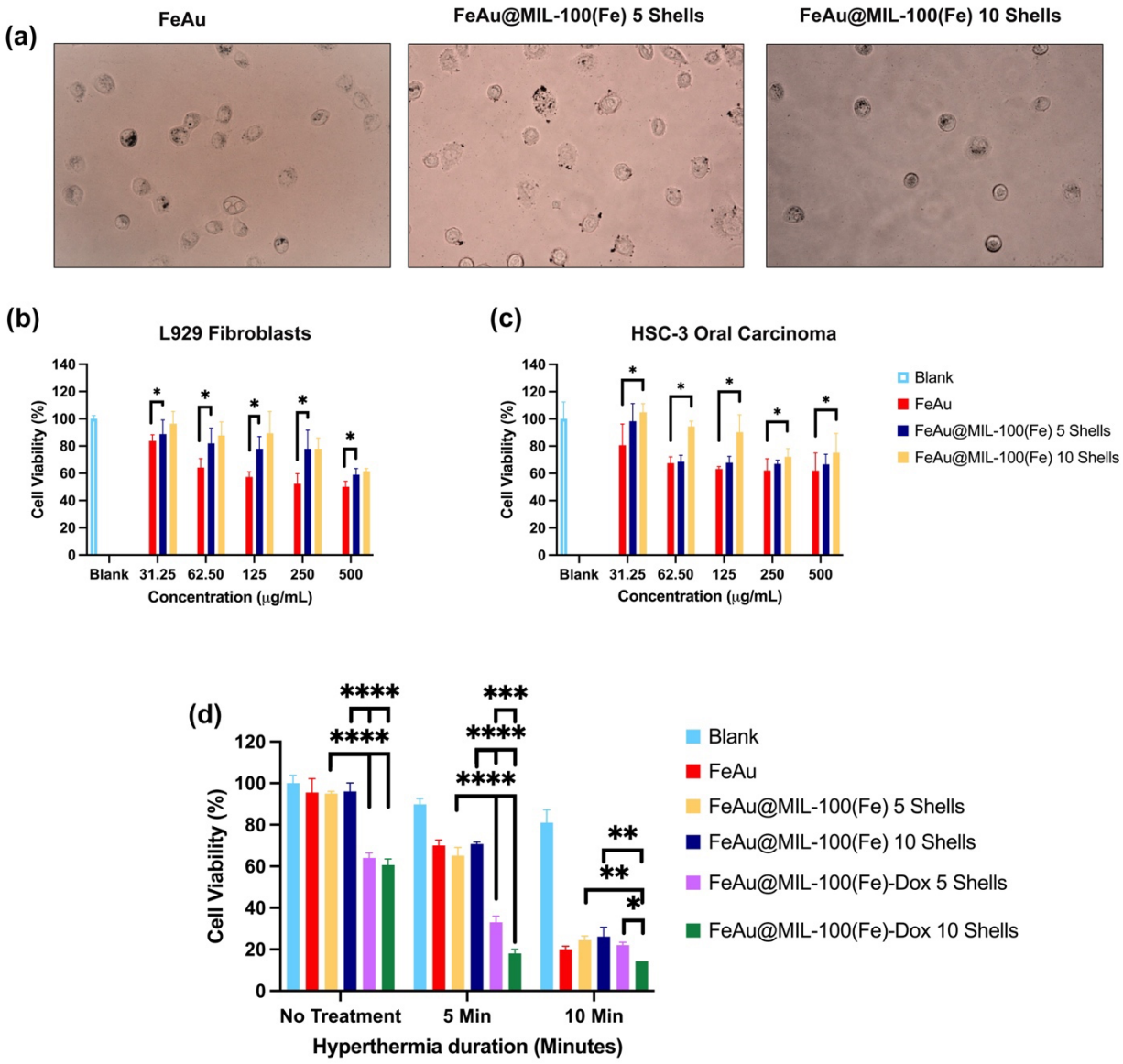


**Figure 4. Analysis of FeAu NPs and FeAu@MOF ingestion and the corresponding effect on cell viability upon hyperthermia treatment. (a)** Optical microscopy images of FeAu, FeAu@MIL-100(Fe) 5 and 10 shells nanostructures. The images show presence of FeAu NPs and FeAu@MOF nanostructures within the cells. The concentration of FeAu nanoparticles is 5 mg/mL **(b)** Cell viability of L929 fibroblasts in the presence of FeAu NPs and FeAu@MOF nanostructures at varying concentrations. **(c)** Cell viability of HSC-3 oral squamous carcinoma cells in the

presence of FeAu NPs and FeAu@MOF nanostructures. Cell viability was assessed using MTT assay. **(d)** Post-hyperthermia **c**ell viability analysis of HSC-3 oral squamous carcinoma cells with or without DOX-encapsulated within FeAu@MOF nanostructures. The graph shows a drastic decrease in cell viability after 10 minutes of hyperthermia treatment.

### 3.6 FeAu@MOF nanostructures improved tumor imaging in an in-vivo mouse model

It has been previously demonstrated that FeAu NPs can serve as suitable negative contrast agents. However, it remained unclear if encapsulation of FeAu NPs within the MOF negatively affected their ability to serve as imaging agent. To investigate this, we performed magnetic resonance imaging (MRI) of tumor-bearing mice administered with PBS or FeAu@MIL-100(Fe) 5, 10 shells nanostructures (Figure 5). The MRI images taken 7 days after hyperthermia treatment displayed enhanced image contrast, facilitating tumor visibility (Figure 5b, c). FeAu@MIL-100 (Fe) enhanced negative image contrast to a higher extent as compared to the control group (Figure 5a). We also acquired MRI images 2 hours after injection of FeAu@MIL-100(Fe) 10 shells nanostructures which clearly highlighted the tumor-affected area, confirming the prospect of using the FeAu@MOF nanostructures for tumor imaging (Figure 5d, e). The tumor volume in FeAu@MIL-100(Fe) 10 shell was also visibly reduced. Collectively, these results suggest that the FeAu@MOF nanostructures may also be employed for simultaneous tumor imaging and therapy, possibly allowing for tumor volume reduction in real-time.

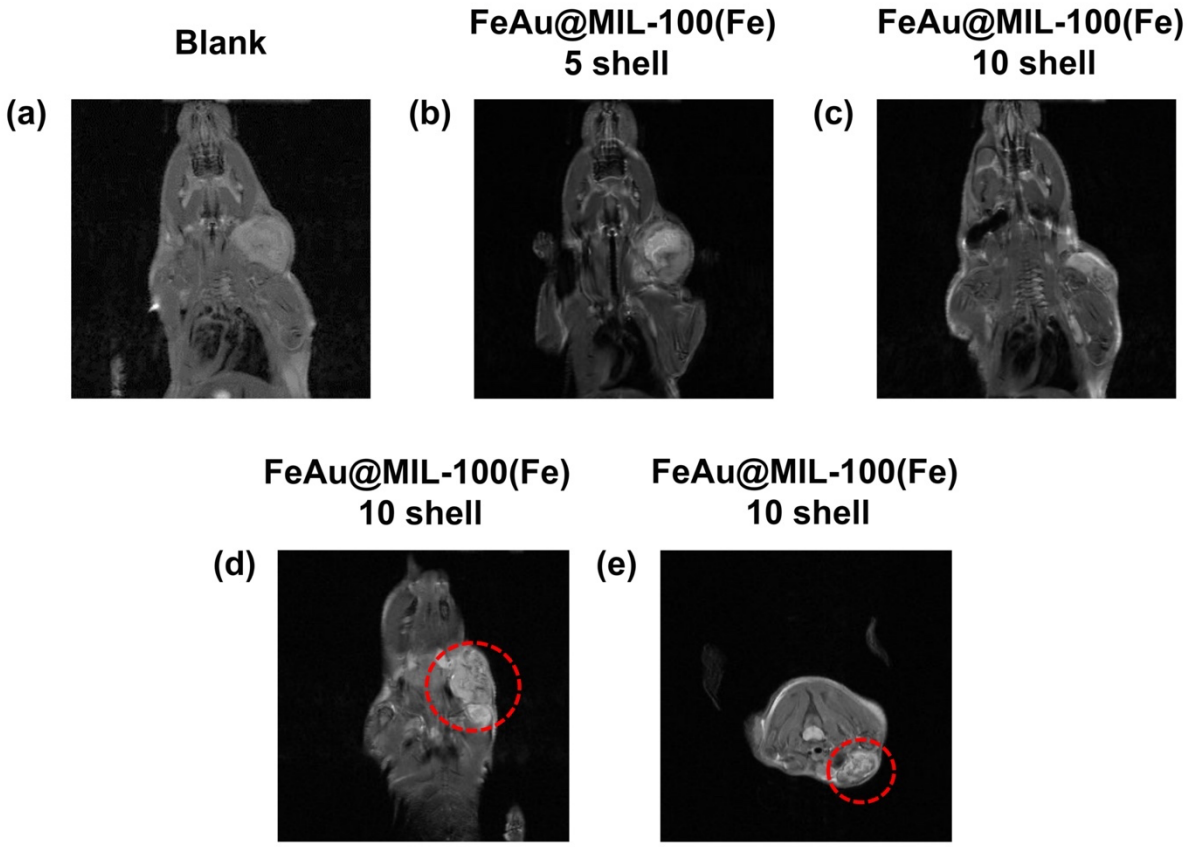


535

536 **Figure 5. Magnetic resonance imaging (MRI) of tumor-bearing mice injected with**
537 **FeAu@MOF nanostructures highlighting application in medical imaging for tumor**
538 **visualization. (a, b and c)** MRI images of tumor-bearing mice injected with PBS, FeAu@MIL-
539 100(Fe) 5 shells nanostructures and FeAu@MIL-100(Fe) 10 shells nanostructures, respectively 7
540 days after treatment. **(d, e)** MRI images of tumor-bearing mice 2 hours after injected with
541 FeAu@MIL-100(Fe) 10 shells nanostructures. The red-colored circles highlight tumor-affected
542 area.

543

544 **3.7 FeAu@MOF nanostructures reduced tumor volume, weight, increase survival time and**
545 **display biological safety to organs in an *in-vivo* mouse model**

A drastic reduction in oral squamous cancer cell viability *in-vitro* motivated us to assess the ability of FeAu@MOF nanostructures in decreasing tumor growth using an *in-vivo* mouse model. To investigate this, mice were divided into three groups namely Control, FeAu@MIL-100(Fe)-Dox 5 shell and FeAu@MIL-100(Fe)-Dox 10 shell (Figure 6a, b). Briefly, both treatment groups comprised of doxorubicin-encapsulated FeAu@MOF nanostructures. Magnetic hyperthermia treatment was performed 2 hours after nanoparticle injection. Tumor volumes were measured over different days. Quantitative analysis of tumor volume highlighted that over 21 days, mice in control groups displayed a consistent increase in the tumor volume, maximizing on day 21 (Figure 6c). The average tumor volume of control group on day 21 was 900 $mm^3$ (Figure 6c). In contrast, the tumors in mice injected with FeAu@MIL-100(Fe)-Dox 5 shell nanostructures first displayed an abrupt increase in tumor volume from day 3 to day 6 followed by a slow yet consistent increase in tumor volume from day 9 to day 21 (Figure 6c). Noteworthy, on day 9, the average tumor volume of this treatment group was lower than the control group, indicating efficacy of hyperthermia-induced doxorubicin released. The lack of significant difference with control group can be attributed to the low encapsulation and release profile of doxorubicin. More importantly, on day 21, the tumor volume of mice injected with FeAu@MIL-100(Fe)-Dox 5 shell nanostructures was 2.5-fold lower as compared to the control group (Figure 6c). Correspondingly, the tumor weight of mice in control group was 800 mg which reduced to half (400 mg) in mice injected with FeAu@MIL-100(Fe)-Dox 5 shell nanostructures (Figure 6d). Most significant decrease in tumor volume as well as weight was displayed by mice injected with FeAu@MIL-100(Fe)-Dox 10 shell nanostructures (Figure 6c). From day 0 to day 21, the tumor volume of mice in this treatment group remained steady. The tumor volume on day 21 was 31 $mm^3$ and the corresponding tumor weight was nearly 10-fold lower (84 mg) than that of mice in the control

group (Figure 6c, d). We then assessed if reduced tumor volume and weight in FeAu@MIL-100(Fe)-Dox 10 shell treatment group translated to an increase survival rate. We observed that after 14 days, the cumulative survival in control group dropped to 0.75 (Figure 6e). This drop was displayed by FeAu@MIL-100(Fe)-Dox 5 shell experimental group after 18 days which can be due to the limited therapeutic efficacy of doxorubicin within the FeAu@MOF nanostructures. After 21 days, the cumulative survival in control group dropped to 0.5 which was similar to that of FeAu@MIL-100(Fe)-Dox 5 shell experimental group (Figure 6e). These data highlight the lack of suitability of 5-shell nanostructures for cancer theranostics. Interestingly, the cumulative survival rate in FeAu@MIL-100(Fe)-Dox 10 shell experimental group was maintained at 1.0 from day 0 to 21 (Figure 6e). The low tumor volume and weight can be an important factor in the survival of mice over 3 weeks. Collectively, these results highlight the high therapeutic efficacy of FeAu@MIL-100(Fe)-Dox 10 shell nanostructures which can be attributed to the successful hyperthermia treatment.

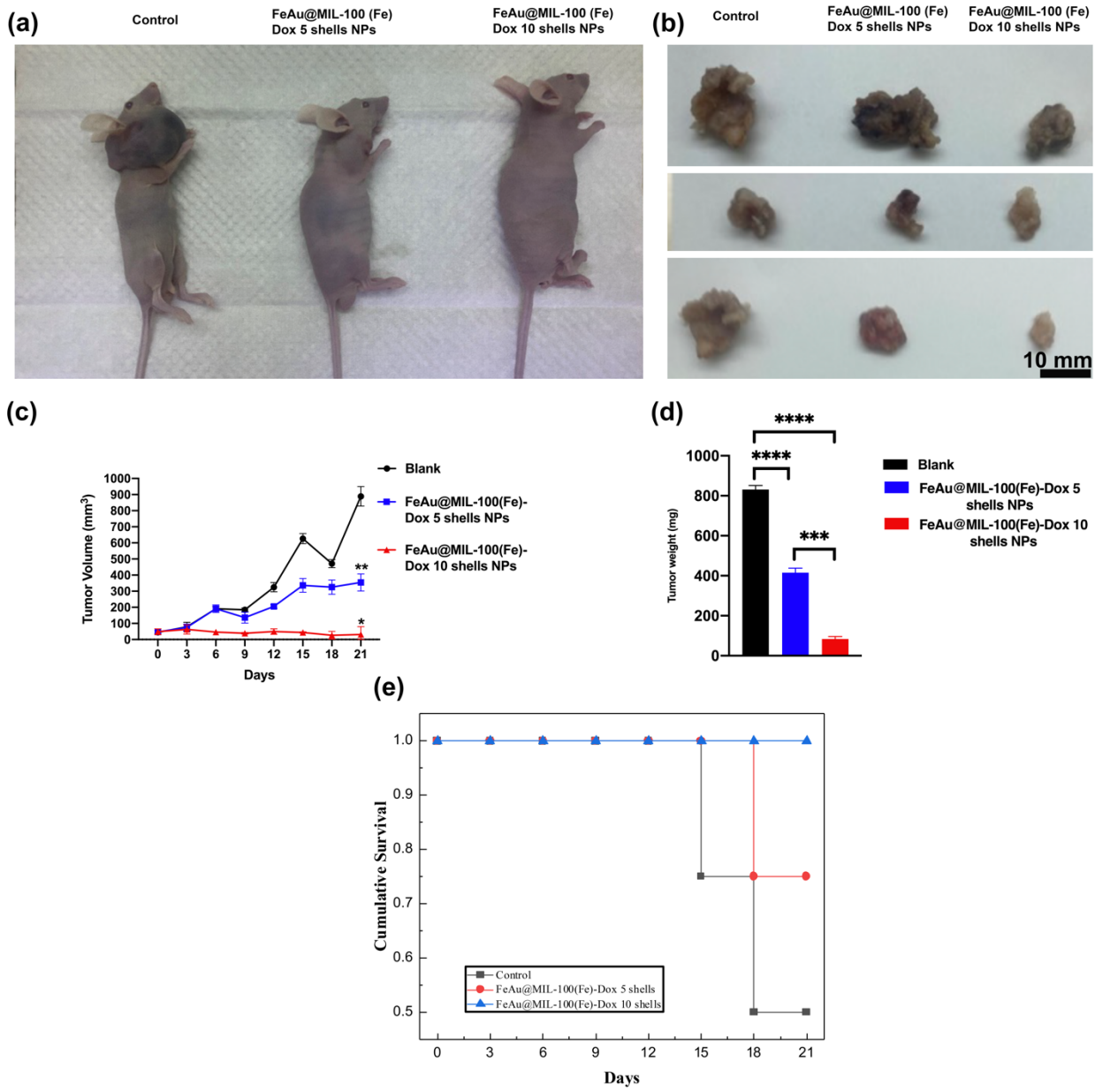


582

583 **Figure 6. Analysis of hyperthermia-induced anti-tumor ability of FeAu@MOF**
584 **nanostructures with 5 and 10 shells using an *in-vivo* mouse model. (a)** Images of tumor-bearing
585 mice injected with PBS, FeAu@MOF nanostructures with 5 and 10 shells after hyperthermia
586 treatment. The control group displayed significantly larger tumor as compared to FeAu@MOF
587 nanostructures. **(b)** Images of tumors dissected from mice treated with PBS, FeAu@MOF
588 nanostructures with 5 and 10 shells after hyperthermia treatment. Mice injected with FeAu@MIL-

100(Fe) 10 shells nanostructures displayed significantly smaller tumors as compared to the control group. 3 biological replicates from each treatment are shown. **(c)** Temporal analysis of tumor volume after injecting mice with FeAu@MOF nanostructures with 5 and 10 shells. **(d)** Analysis of tumor weight after injecting tumor-bearing mice with PBS, FeAu@MIL-100(Fe) 5 and 10 shells nanostructures, followed by hyperthermia treatment. **(e)** Cumulative survival rate analysis of mice after administration with FeAu@MIL-100(Fe) 5 and 10 shells nanostructures followed by hyperthermia treatment. Statistical analysis of tumor volume was performed using Kruskal-Wallis test with Dunn's multiple comparisons and statical analysis of tumor weight was performed using one-way ANOVA test using GraphPad Prism (Version 9).

We also performed Immunohistochemical staining (H&E staining) of major organs of mice in control and different treatment groups to assess the safety of this nanotheranostics platform (Figure 7). Cellular morphology was studied which can highlight necrotic areas. Our findings showed that FeAu@MIL-100(Fe) and FeAu@MIL-100(Fe)-Dox 10 shells treatment groups did not display signs of significant organ damage as compared to the control group, demonstrating the suitability of this platform for therapeutic applications.

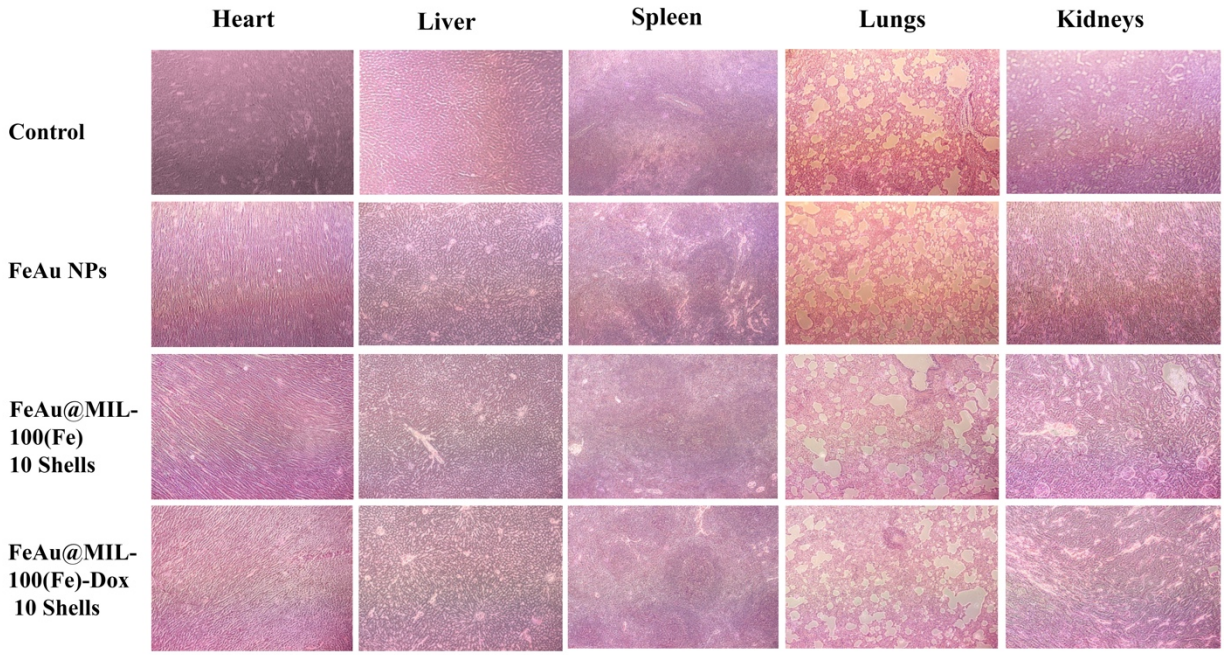


**Figure 7. Assessment of anatomical safety via Immunohistochemical analysis of vital organs of mice using Hematoxylin and Eosin (H&E) staining displayed lack of significant damage to heart, liver, spleen, lungs and kidneys.**

In this study, FeAu@MIL-100(Fe) MOF nanostructures are synthesized and their applications in medical imaging and cancer theranostics are explored. The addition of MOF shells around FeAu NPs improved the biocompatibility and provided opportunity for DOX encapsulation for cancer treatment. The FeAu@MOF nanostructures enhanced negative image contrast of cancer tissue and facilitated in medical imaging even 7 days after injection. Furthermore, hyperthermia treatment resulted in 90% apoptosis of oral squamous cancer cells. Upon hyperthermia treatment, Dox-encapsulated FeAu@MOF nanostructures drastically reduced tumor volume, weight, improved cumulative survival rate and insignificant damage to major organs in an *in-vivo* mouse model.

Collectively, these findings highlight potential of FeAu@MOF theranostic platform for cancer tissue visualization and eradication.

## Acknowledgements

Technical assistance from the Precision Analysis and Material Research Center of National Taipei University of Technology (Taipei Tech) is appreciated. Technical assistance from Instrumentation Center of National Taiwan University with the SQUID is appreciated.

## Funding

The authors are grateful for the financial supports of this research by the Ministry of Science and Technology of Taiwan (MOST 108-2628-E-027-003-MY3; MOST 111-2221-E-027-105), the National Taipei University of Technology-Mackay Memorial Hospital Joint Research Program (NTUT-MMH-108-08, NTUT-MMH-109-04, NTUT-MMH-111-01).

## Author contributions

**Udesh Dhawan:** Writing - Original Draft, Writing - Review & Editing, Methodology, Formal analysis, Data Curation, Visualization. **Ching-Li Tseng:** Writing - Review & Editing, Methodology, Funding acquisition. **Ping-Hsuan Wu:** Investigation, Formal analysis, Data Curation, Validation. **Mei-Yi Liao:** Resources. **Huey-Yuan Wang:** Writing - Review & Editing, Conceptualization, Methodology, Project administration, Funding acquisition. **Kevin C.-W. Wu:** Conceptualization, Methodology, Supervision, Writing - Review & Editing. **Ren-Jei Chung:** Conceptualization, Methodology, Supervision, Project administration, Funding acquisition, Writing - Review & Editing.

## References


A. Le Campion, C. M. B. Ribeiro, R. R. Luiz, F. F. da Silva Junior, H. C. S. Barros, K. C. B. Dos Santos, et al., **Low Survival Rates of Oral and Oropharyngeal Squamous Cell Carcinoma**. *Int J Dent*. 2017;2017:5815493

B. Wang, S. Zhang, K. Yue and X. D. Wang, **The recurrence and survival of oral squamous cell carcinoma: a report of 275 cases**. *Chin J Cancer*. 2013;32:614-8

L. Hartner, **Chemotherapy for Oral Cancer**. *Dent Clin North Am*. 2018;62:87-97

J. A. Bonner, P. M. Harari, J. Giralt, N. Azarnia, D. M. Shin, R. B. Cohen, et al., **Radiotherapy plus cetuximab for squamous-cell carcinoma of the head and neck**. *N Engl J Med*. 2006;354:567-78

J. S. Durham, P. Brasher, D. W. Anderson, J. Yoo, R. Hart, J. C. Dort, et al., **Effect of Fluorescence Visualization-Guided Surgery on Local Recurrence of Oral Squamous Cell Carcinoma: A Randomized Clinical Trial**. *JAMA Otolaryngol Head Neck Surg*. 2020;146:1149-1155

S. Minhas, M. Kashif, W. Altaf, N. Afzal and A. H. Nagi, **Concomitant-chemoradiotherapy-associated oral lesions in patients with oral squamous-cell carcinoma**. *Cancer Biol Med*. 2017;14:176-182

H. Kawachi, Y. Aoyagi, K. Ito, K. Saito, K. Sato, S. Ogane, et al., **Two cases of oral squamous cell carcinoma that achieved complete response through interstitial hyperthermia after the patients refused surgery**. *J Oral Max Surg Med*. 2020;32:387-393

Y. Q. Li, M. Xu, U. Dhawan, W. C. Liu, K. T. Wu, X. R. Liu, et al., **Iron-gold alloy nanoparticles serve as a cornerstone in hyperthermia-mediated controlled drug release for cancer therapy**. *Int J Nanomed*. 2018;13:5499-5509

S. P. C. Hsu, U. Dhawan, Y. Y. Tseng, C. P. Lin, C. Y. Kuo, L. F. Wang, et al., **Glioma-sensitive delivery of Angiopep-2 conjugated iron gold alloy nanoparticles ensuring simultaneous tumor imaging and hyperthermia mediated cancer theranostics**. *Applied Materials Today*. 2020;18

S. Kwiatkowski, B. Knap, D. Przystupski, J. Saczko, E. Kedzierska, K. Knap-Czop, et al., **Photodynamic therapy - mechanisms, photosensitizers and combinations**. *Biomed Pharmacother*. 2018;106:1098-1107

R. B. Mikkelsen and P. Wardman, **Biological chemistry of reactive oxygen and nitrogen and radiation-induced signal transduction mechanisms**. *Oncogene*. 2003;22:5734-54

A. Lak, S. Disch and P. Bender, **Embracing Defects and Disorder in Magnetic Nanoparticles**. *Adv Sci (Weinh)*. 2021;8:2002682

Y. Q. Li, D. Dhawan, H. Y. Wang, X. R. Liu, H. H. Ku, M. T. Tsai, et al., **Theranostic Iron@Gold Core-Shell Nanoparticles for Simultaneous Hyperthermia-Chemotherapy upon Photo-Stimulation**. *Part Part Syst Char*. 2019;36

U. Dhawan, C. L. Tseng, H. Y. Wang, S. Y. Hsu, M. T. Tsai and R. J. Chung, **Assessing Suitability of Co@Au Core/Shell Nanoparticle Geometry for Improved Theranostics in Colon Carcinoma**. *Nanomaterials-Basel*. 2021;11

S. K. Sohaebuddin, P. T. Thevenot, D. Baker, J. W. Eaton and L. Tang, **Nanomaterial cytotoxicity is composition, size, and cell type dependent**. *Particle and Fibre Toxicology*. 2010;7:22

C. K. Ting, U. Dhawan, C. L. Tseng, C. S. Y. A. Gong, W. C. Liu, H. D. Tsai, et al., **Hyperthermia-Induced Controlled Local Anesthesia Administration Using Gelatin-Coated Iron-Gold Alloy Nanoparticles**. *Pharmaceutics*. 2020;12

T. S. Anilkumar, Y. J. Lu and J. P. Chen, **Optimization of the Preparation of Magnetic Liposomes for the Combined Use of Magnetic Hyperthermia and Photothermia in Dual Magneto-Photothermal Cancer Therapy**. *Int J Mol Sci*. 2020;21

M. Salimi, S. Sarkar, R. Saber, H. Delavari, A. M. Alizadeh and H. T. Mulder, **Magnetic hyperthermia of breast cancer cells and MRI relaxometry with dendrimer-coated iron-oxide nanoparticles**. *Cancer Nanotechnol*. 2018;9

J. H. Man, J. D. Shoemake, T. P. Ma, A. E. Rizzo, A. R. Godley, Q. L. Wu, et al., **Hyperthermia Sensitizes Glioma Stem-like Cells to Radiation by Inhibiting AKT Signaling**. *Cancer Res*. 2015;75:1760-1769

Y. J. Sun, L. W. Zheng, Y. Yang, X. Qian, T. Fu, X. W. Li, et al., **Metal-Organic Framework Nanocarriers for Drug Delivery in Biomedical Applications**. *Nano-Micro Lett*. 2020;12

L. Wang, M. Zheng and Z. G. Xie, **Nanoscale metal-organic frameworks for drug delivery: a conventional platform with new promise**. *J Mater Chem B*. 2018;6:707-717

J. Feng, W.-X. Ren, F. Kong and Y.-B. Dong, **Recent insight into functional crystalline porous frameworks for cancer photodynamic therapy**. *Inorg Chem Front*. 2021;8:848-879

X. F. Zhong and X. Sun, **Nanomedicines based on nanoscale metal-organic frameworks for cancer immunotherapy**. *Acta Pharmacol Sin*. 2020;41:928-935

M. Levy, C. Wilhelm, J. M. Siaugue, O. Horner, J. C. Bacri and F. Gazeau, **Magnetically induced hyperthermia: size-dependent heating power of gamma-Fe2O3 nanoparticles**. *J Phys-Condens Mat*. 2008;20

D. Yang, J. Xu, G. Yang, Y. Zhou, H. Ji, H. Bi, et al., **Metal-organic frameworks join hands to create an anti-cancer nanoplatform based on 808 nm light driving up-conversion nanoparticles**. *Chem Eng J*. 2018;344:363-374

A. Ashkenazi and V. M. Dixit, **Death receptors: signaling and modulation**. *Science*. 1998;281:1305-8

H. Demirci, N. Slimani, M. Pawar, R. E. Kumon, P. Vaishnava and C. G. Besirli, **Magnetic Hyperthermia in Y79 Retinoblastoma and ARPE-19 Retinal Epithelial Cells: Tumor Selective Apoptotic Activity of Iron Oxide Nanoparticle**. *Transl Vis Sci Technol*. 2019;8:18